Supplemental Materials

Molecular Biology of the Cell

Masucci *et al*.

SUPPLEMENTARY FIGURE LEGENDS

Figure S1

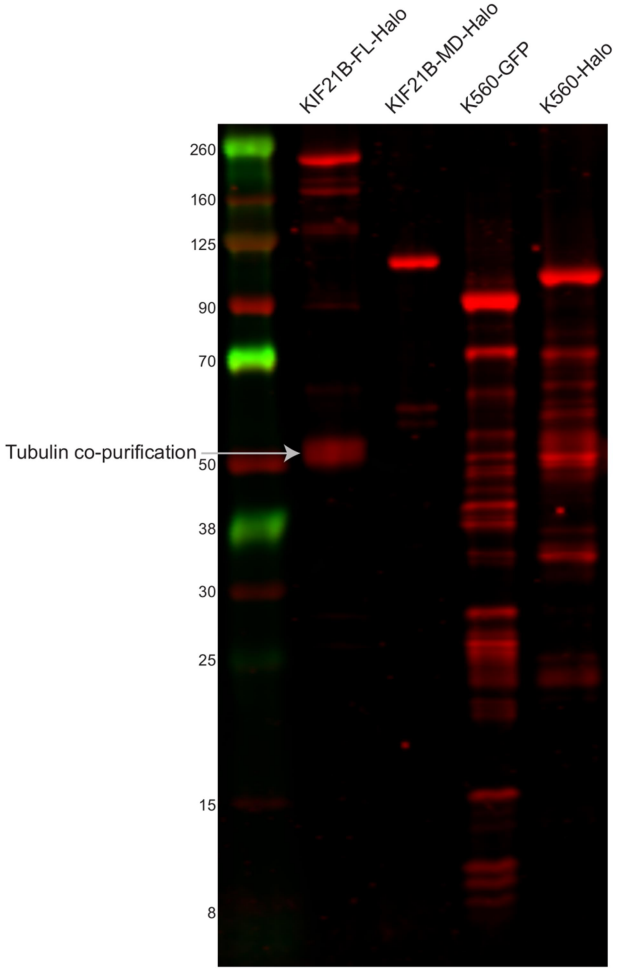

Figure S1. Western blot analysis of recombinant proteins. Revert 700 Total Protein Stain of purified kinesin proteins. 10 µL of 1-2 µM protein was loaded per lane.

Figure S2

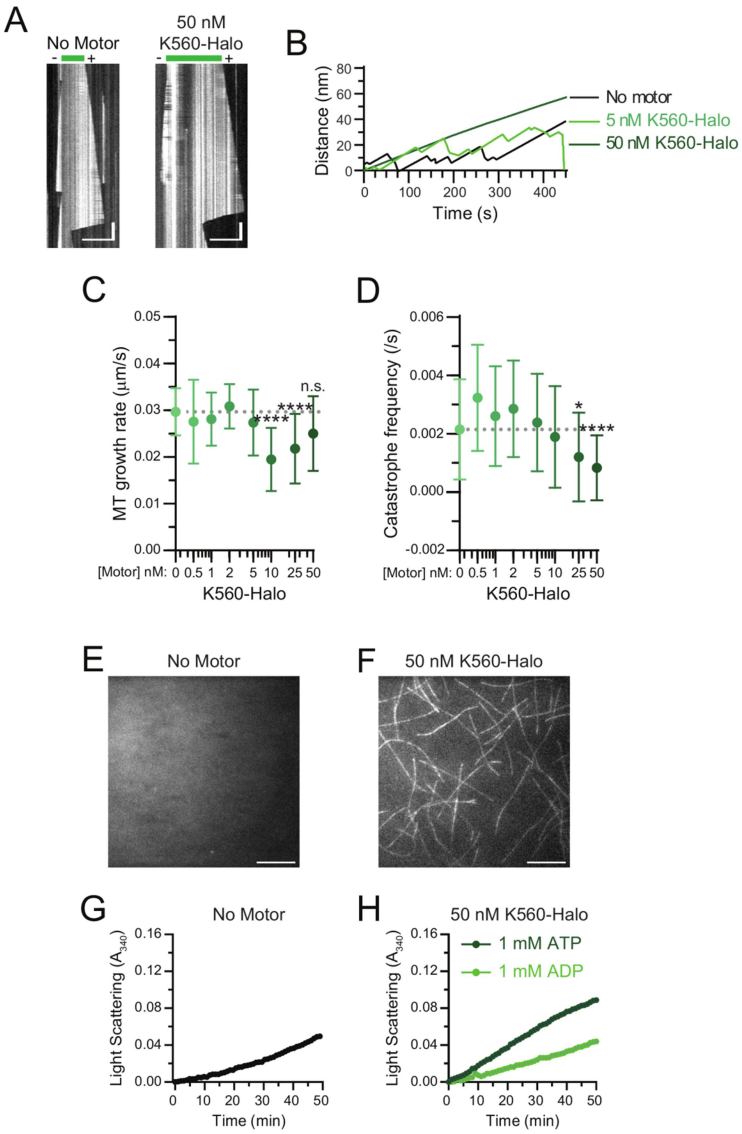

Figure S2. K560 motors stabilize MT dynamics and promote MT assembly. A) Kymographs showing dynamic MTs polymerizing from stabilized MT seeds in the absence or presence of K560-Halo. Plot for the no motor condition was repeated from figure 1 for comparison. Scale bars: 10 µm (horizontal) and 30 s (vertical). B) Average MT plus-end

growth trace. For each condition 10 MT plus-end trajectories were averaged. C) MT plus-end growth speed in the presence of increasing concentrations of K560-Halo. Plotted are means and standard deviations. Kruskal–Wallis one-way ANOVA and Dunn's multiple comparison (n.s. $p > 0.05$; ****$p < 0.0001$). D) MT plus-end catastrophe frequency in the presence of increasing concentrations of K560-GFP. Plotted are mean and standard deviations. Kruskal–Wallis one-way ANOVA and Dunn's multiple comparison (*$p < 0.05$; ****$p < 0.0001$). E-F) TIRF microscopy images of free tubulin dimers incubated in the absence or presence of 50 nM K560-Halo. Images were taken 10 min after solutions were added and incubated in flow chambers. Scale bar: 10 μm. G-H) Light scattering traces for solutions containing buffer, MT polymerizing and depolymerizing drugs, 50 nM K560-Halo with 1 mM ATP or 1 mM ADP. Graphs show mean values for each time point (See Figure S3 for graphs with standard deviations). Means were compared with Kruskal–Wallis one-way ANOVA and Dunn's multiple comparison. (Buffer – K560-Halo ****$p < 0.0001$; K560-Halo ATP – K560-Halo ADP ****$p < 0.0001$). Data from 7-18 traces from N = 5 independent experiments. Unless otherwise indicated, data from 51-74 MTs and N = 4-5 independent experiments.

Figure S3

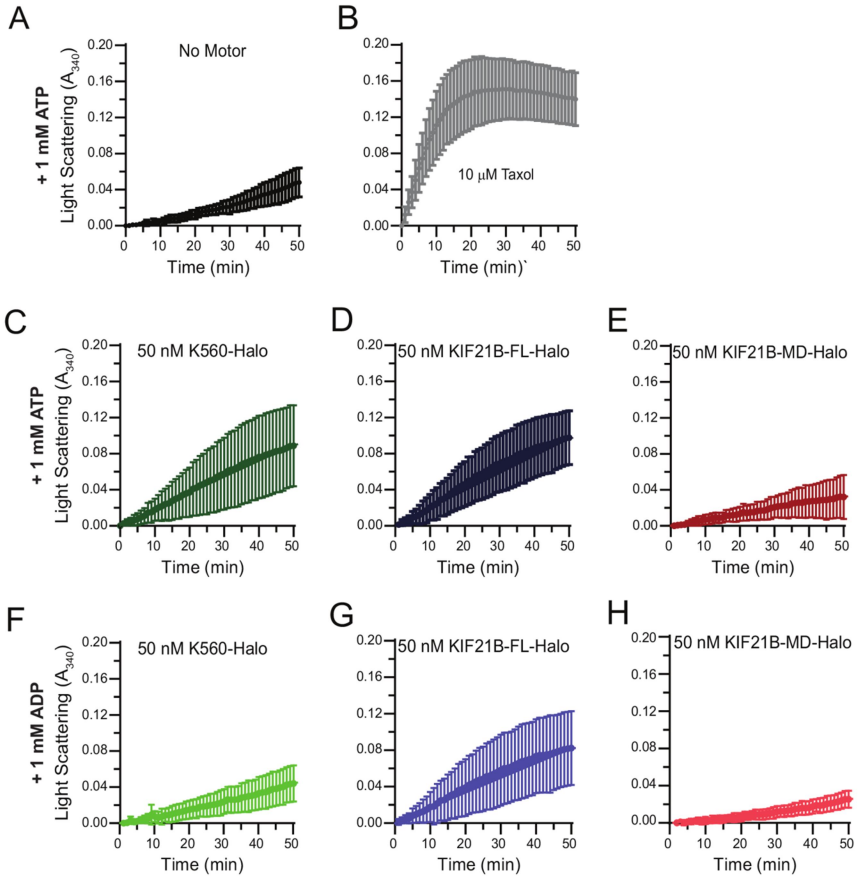

Figure S3. KIF21B C-terminal MTRs promote MT assembly. Light scattering traces for solutions containing buffer, MT polymerizing and depolymerizing drugs, or kinesin motors with 1 mM ATP or 1 mM ADP. Graphs show mean values and standard deviations for each

time point. Means were compared with Kruskal–Wallis one-way ANOVA and Dunn's multiple comparison. Data from 7-22 traces from N = 5 independent experiments.

Figure S4

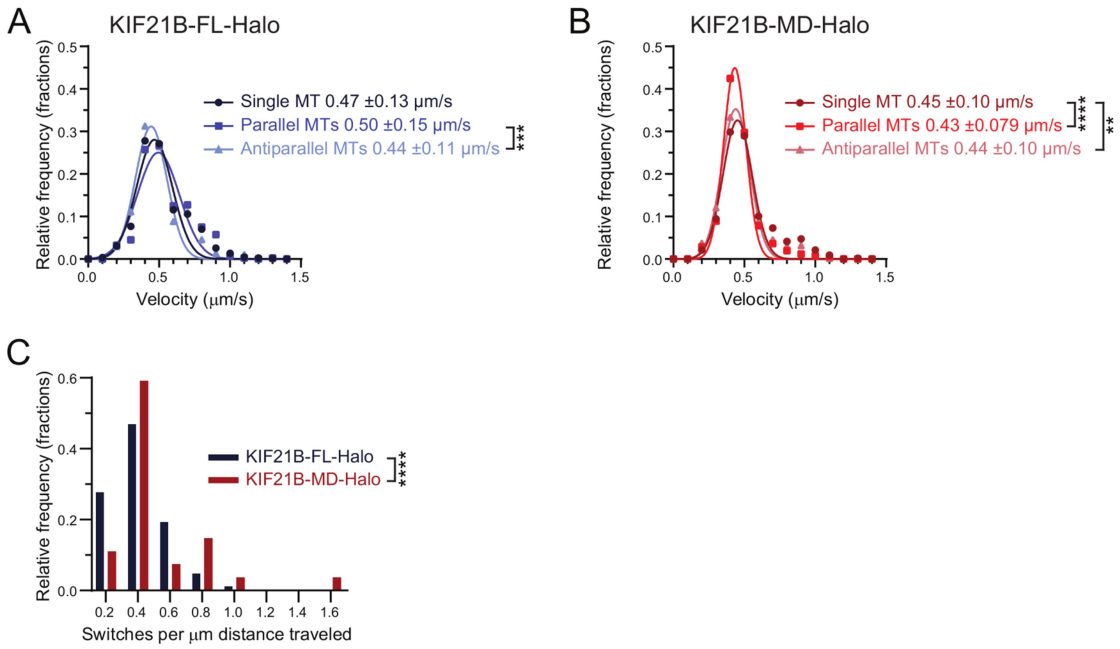

Figure S4. KIF21B MTBs promote track switching, but do not affect motor velocity. A and B) Histogram of velocities of single KIF21B-FL-Halo and KIF21B-MD-Halo molecules along single MTs or MT bundles. Data points were fitted by a gaussian function. Listed are the means and standard deviations. Ordinary one-way ANOVA (**p < 0.01; ***p < 0.001; ****p < 0.0001). C) Histogram of the number of track switches per distance traveled along antiparallel MTs for KIF21B-FL-Halo and KIF21B-MD-Halo motors. Two-tailed Mann-Whitney (****p < 0.0001). Data from 400-1069 motor runs from n = 20-60 MTs and N = 6-7 independent experiments.

Figure S5

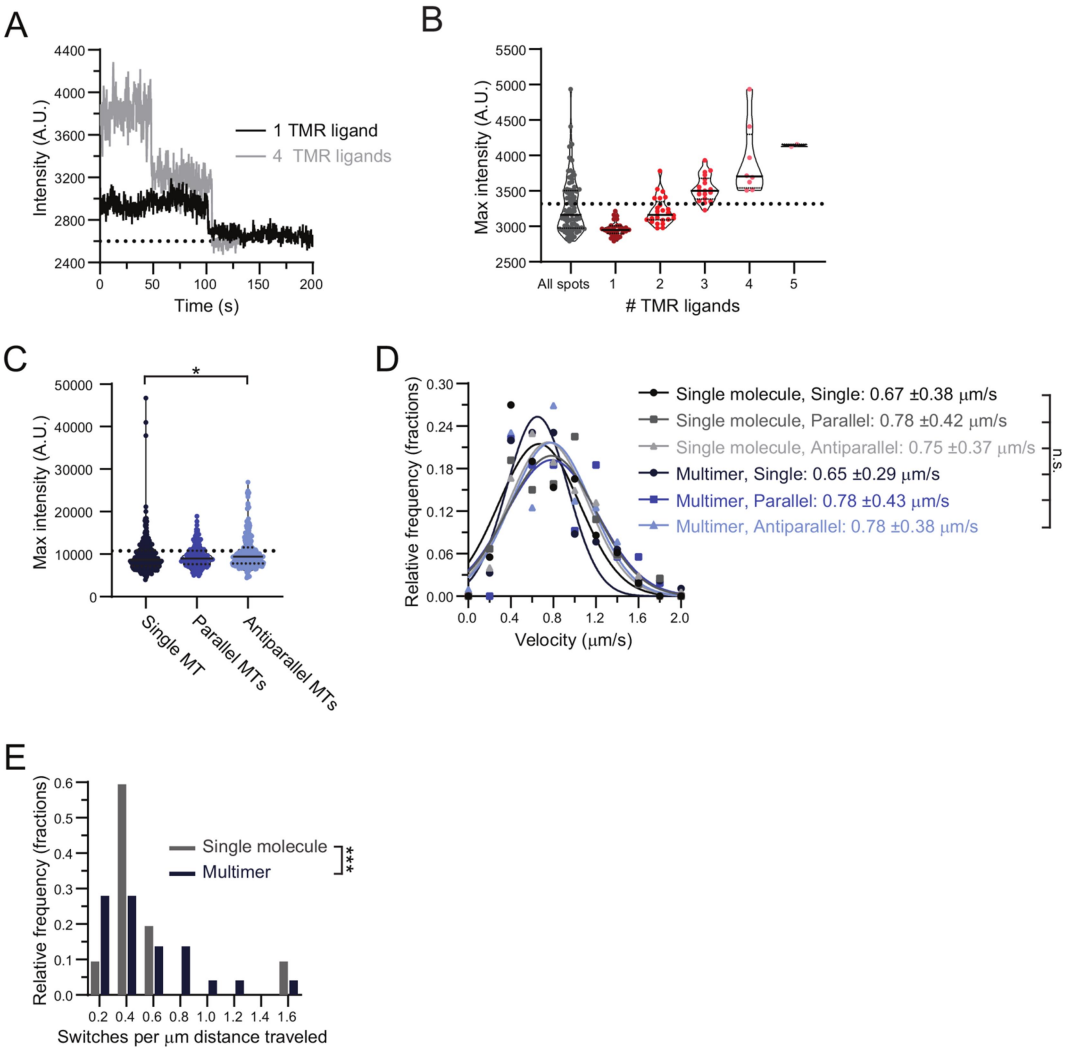

Figure S5. Calibration of single molecule and multimer intensity threshold and velocity quantification for purified KIF21B motors in low ionic strength conditions. A) Example intensity profiles for TMR Halo ligand quenching on KIF21B-FL-Halo motors. Black traces indicate quenching of one TMR dye and gray traces indicate quenching of four TMR

molecules. Dashed black line represents average background intensity (2,632 A.U.). B) Maximum intensity distribution of KIF21B spots versus distributions representing increasing TMR dye number. The threshold separation between 2 and 3 TMR molecules is indicated with the black dashed line (3,343 A.U.). Plotted are individual values in color and means in solid black lines and 25^{th} and 75^{th} quartiles in dotted black lines. Data from 2-83 motor runs from n = 20 MTs and N = 1 independent experiment. C) Maximum intensity distribution of KIF21B particles moving on different MT types. The threshold for single molecule intensity is indicated with the black dashed line (10,117 A.U.). Plotted are individual values in color and means in solid black lines and 25^{th} and 75^{th} quartiles in dotted black lines. Ordinary one-way ANOVA (*$p < 0.05$). Data from 54-174 motor runs from n = 11-12 MTs and N = 4 independent experiments, unless otherwise stated. D) Histogram of velocities of single molecule and multimeric KIF21B-FL-Halo motors along single MTs or MT bundles. Data points were fitted by a gaussian function. Listed are the means and standard deviations. Ordinary one-way ANOVA (n.s. > 0.05). E) Histogram of the number of track switches per distance traveled along antiparallel MTs for single molecule and multimeric KIF21B-FL-Halo motors. Two-tailed Mann-Whitney (***$p < 0.001$). Unless otherwise stated, data for single and multimeric KIF21B-FL-Halo from 54-174 motor runs from n = 11-12 MTs and N = 4 independent experiments.

Figure S6

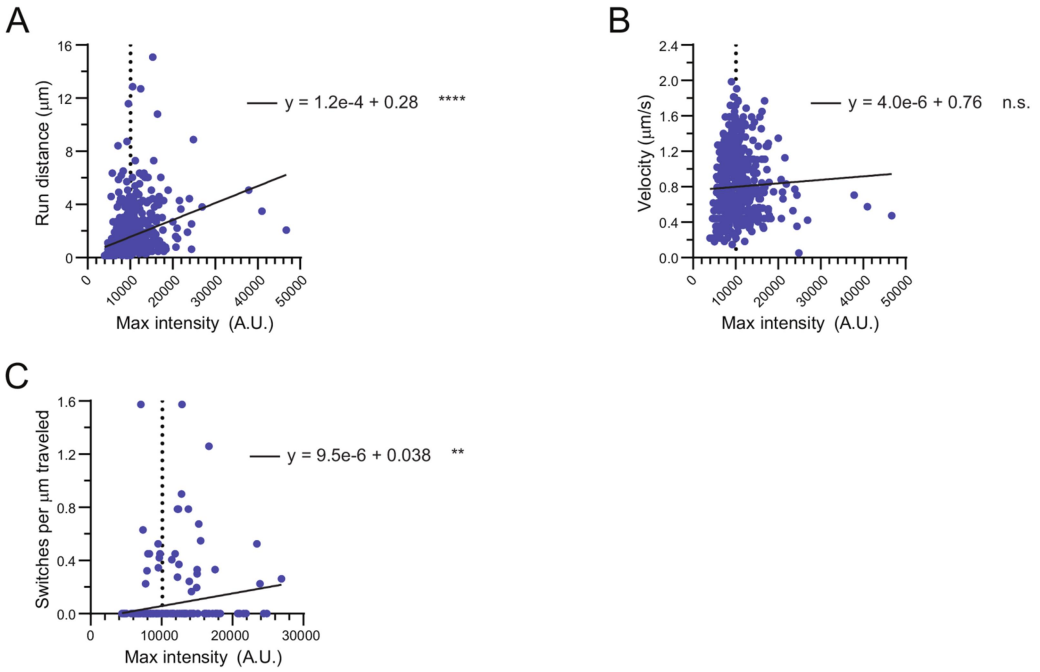

Figure S6. KIF21B motor intensity is positively correlated with run distance and track switching, and not correlated with velocity. A) Scatter plot of maximum motor intensity versus run distance. Plotted is a linear regression line for KIF21B-FL-Halo motors. Black dashed line indicates intensity threshold for single molecules. F test (****p < 0.0001). B)

Scatter plot of maximum motor intensity versus velocity. Plotted is a linear regression line for KIF21B-FL-Halo motor spots. Black dashed line indicates intensity threshold for single molecules. F test (n.s. $p > 0.05$). C) Scatter plot of maximum motor intensity versus switches per run distance. Plotted is a linear regression line for KIF21B-FL-Halo spots. Black dashed line indicates intensity threshold for single molecules. F test (** $p < 0.01$). Data from 54-174 motor runs from n = 11-12 MTs and N = 4 independent experiments.

Figure S7

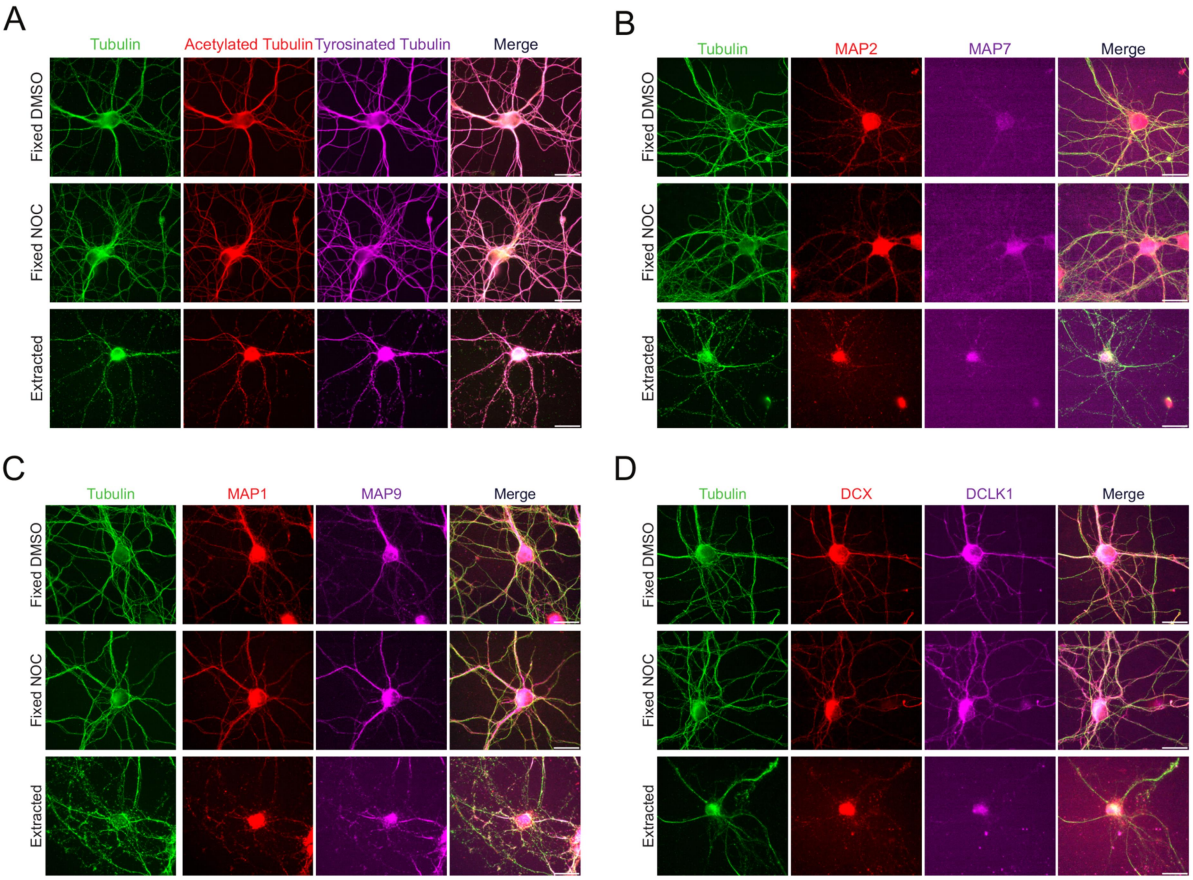

Figure S7. Tubulin PTMs are maintained on extracted MT arrays from cultured hippocampal neurons. A-D) Representative widefield images of fixed or extracted hippocampal neurons stained for tubulin and dendritic tubulin PTMs and MAPs. Brightness and contrast levels are adjusted differently for each image. Scale bars: 25 μm.

Figure S8

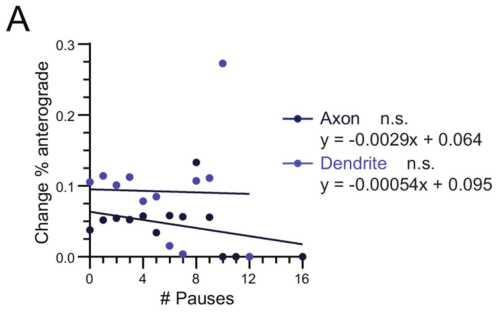

Figure S8. Motor pausing along extracted dendritic MT arrays is not correlated with track switches. Correlation between number of pauses and change in percentage of retrograde segments. Data was fitted with simple linear regression lines. F test (n.s. p >

0.05). Data from 59-80 processes from n = 49-50 neurons and N = 4 independent experiments.

Figure S9

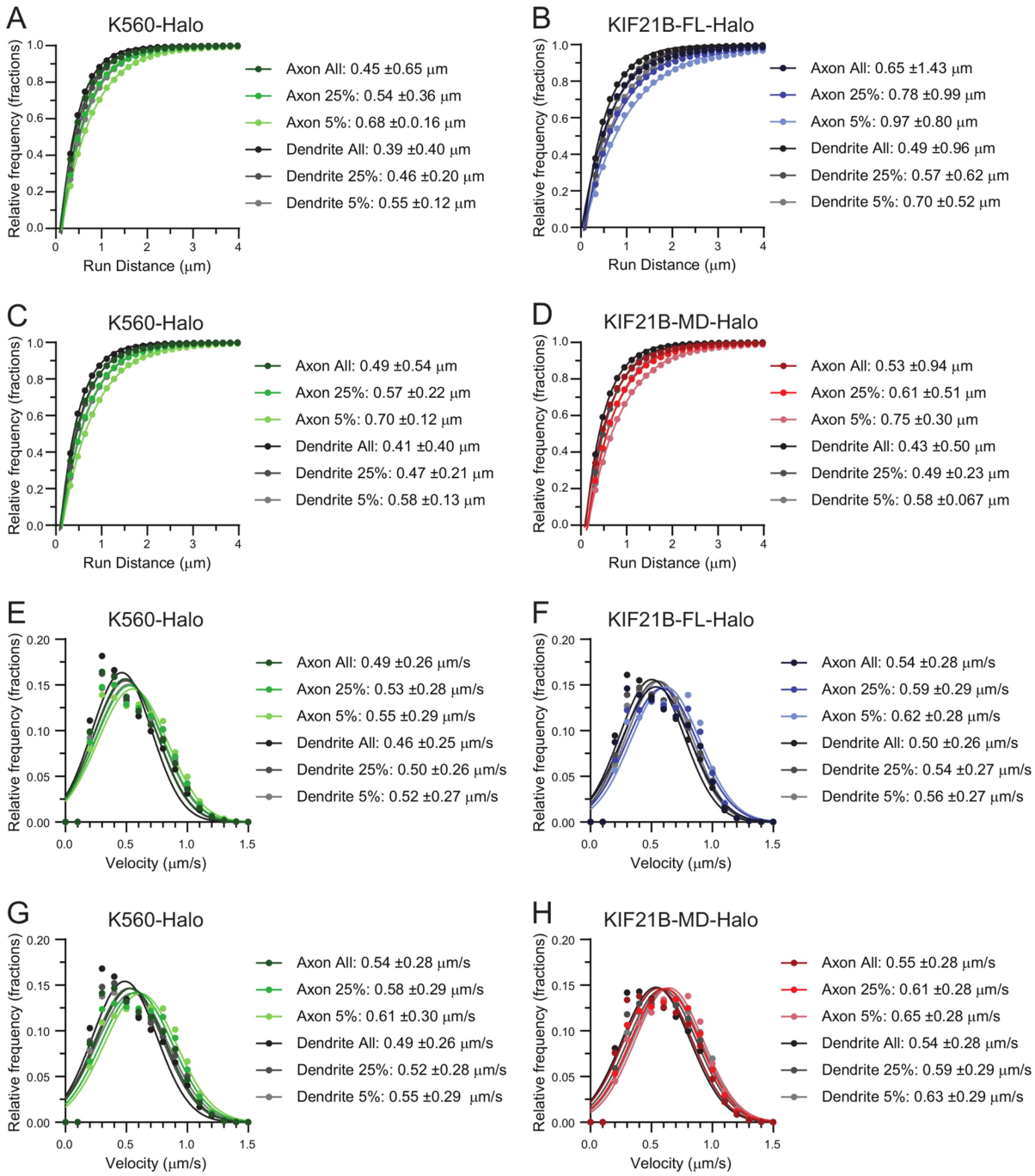

Figure S9. Kinesin motility is affected by MT arrangement and motor multimerization. A-D) Cumulative distribution of total distance K560-GFP and KIF21B-FL-Halo or KIF21B-MD-Halo motors traveled along extracted MT arrays in axons and dendrites. Data points were fitted by a single exponential decay function. Listed are the average distance traveled, as calculated by taking the inverse of the rate constant, and standard deviations. E-H) Histogram of velocities of motors along different MT bundles. Data points were fitted by a gaussian function. Listed are the means and standard deviations. Data from 24-42 processes from n = 21-28 neurons and N = 4 independent experiments.

Figure S10

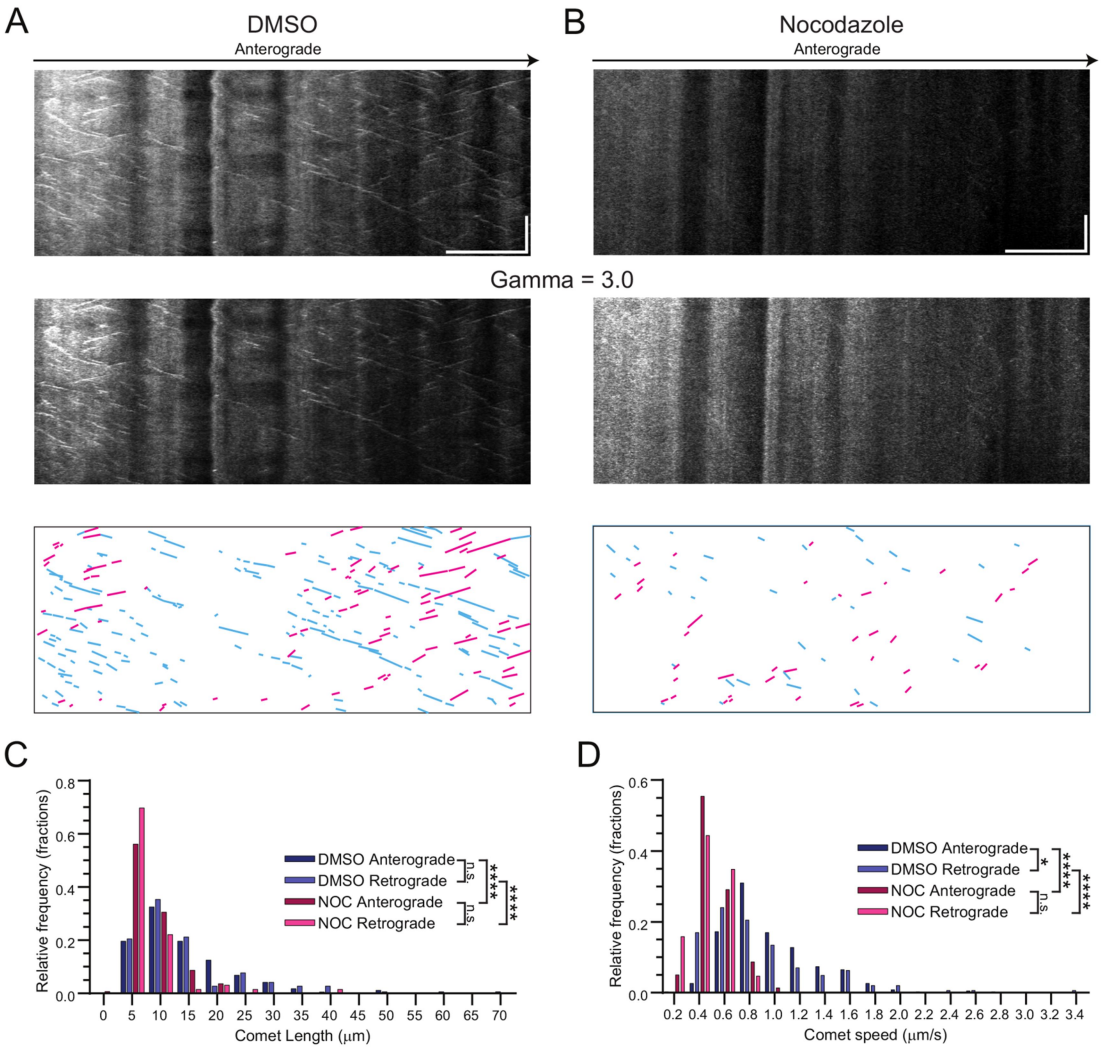

Figure S10. Low dose nocodazole reduced EB3 dynamics in dendrites od live neurons. A and B) Representative kymographs of EB3 comets in dendrites of live neurons treated with DMSO or low dose nocodazole (100 nM), followed by gamma enhanced images and EB3 comet tracing diagrams. Scale bars: 10 μm (horizontal) and 2 min (vertical). B)

Histogram of EB3 comet run lengths. Motor and DMSO or nocodazole (Noc) conditions as well as comet direction are indicated in the legend. Listed for each condition is the average distance traveled, as calculated by taking the inverse of the rate constant, and standard deviations from a fitted single exponential decay function. Kruskal–Wallis one-way ANOVA and Dunn's multiple comparison (n.s. $p > 0.05$, ****$p < 0.0001$). C) Histogram of EB3 comet velocities. Motor and DMSO or nocodazole (Noc) conditions are indicated in the legend. Data points were fitted by a gaussian function. Listed are the means and standard deviations from a fitted gaussian function for each condition. Kruskal–Wallis one-way ANOVA and Dunn's multiple comparison (n.s. $p > 0.05$., *$p < 0.05$, ****$p < 0.0001$). Data from 63-476 comets from n = 6 neurons and N = 3 independent experiments.

Figure S11

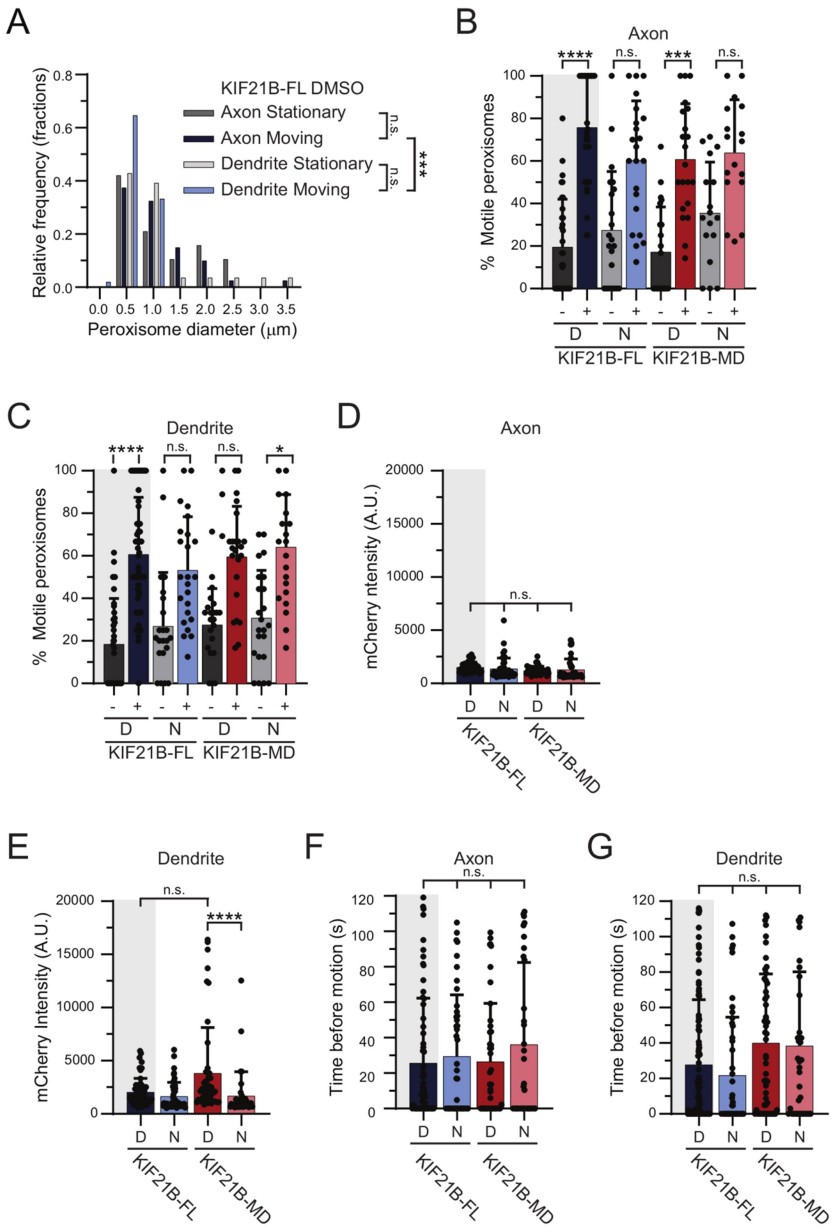

Figure S11. Induced recruitment of KIF21B motors to peroxisome cargo in live neurons promotes cargo movement. A) Histogram of KIF21B-FL recruited peroxisome diameter measured along axis of axons or dendrites that move post photoactivation or remain stationary in DMSO conditions. Kruskal–Wallis one-way ANOVA and Dunn's multiple

comparison (n.s. $p > 0.05$; ***$p < 0.001$). Data from 40-51 peroxisomes from n = 16-23 neurons and N = 3 independent experiments. B and C) Percentage of peroxisomes that are motile in axons and dendrites with and without photoactivation. Data for KIF21B-FL DMSO is repeated here from Figure 5 for comparison and marked with gray shading. DMSO (D) or nocodazole (N) conditions are indicated at the bottom of the graph. Plotted are means and standard deviations. Kruskal–Wallis one-way ANOVA and Dunn's multiple comparison (n.s. $p > 0.05$; *$p < 0.05$; ***$p < 0.001$; ****$p < 0.0001$). D and E) Intensity of mCherry signal on moving peroxisomes with recruitment of KIF21B-FL or -MD. DMSO (D) or nocodazole (N) conditions are indicated at the bottom of the graph. Means and standard deviations are plotted. Kruskal–Wallis one-way ANOVA and Dunn's multiple comparison (n.s. $p > 0.05$; ****$p < 0.0001$). F and G) Time taken by peroxisomes to begin movement post photoactivation in axons and dendrites. Data for KIF21B-FL DMSO is repeated here from Figure 5 for comparison and marked with gray shading. DMSO (D) or nocodazole (N) conditions are indicated at the bottom of the graph. Means and standard deviations are reported. Kruskal–Wallis one-way ANOVA and Dunn's multiple comparison (n.s. $p > 0.05$). Unless otherwise stated, data from 37-120 peroxisomes from n = 18-52 neurons and N = 3-6 independent experiments.

Figure S12

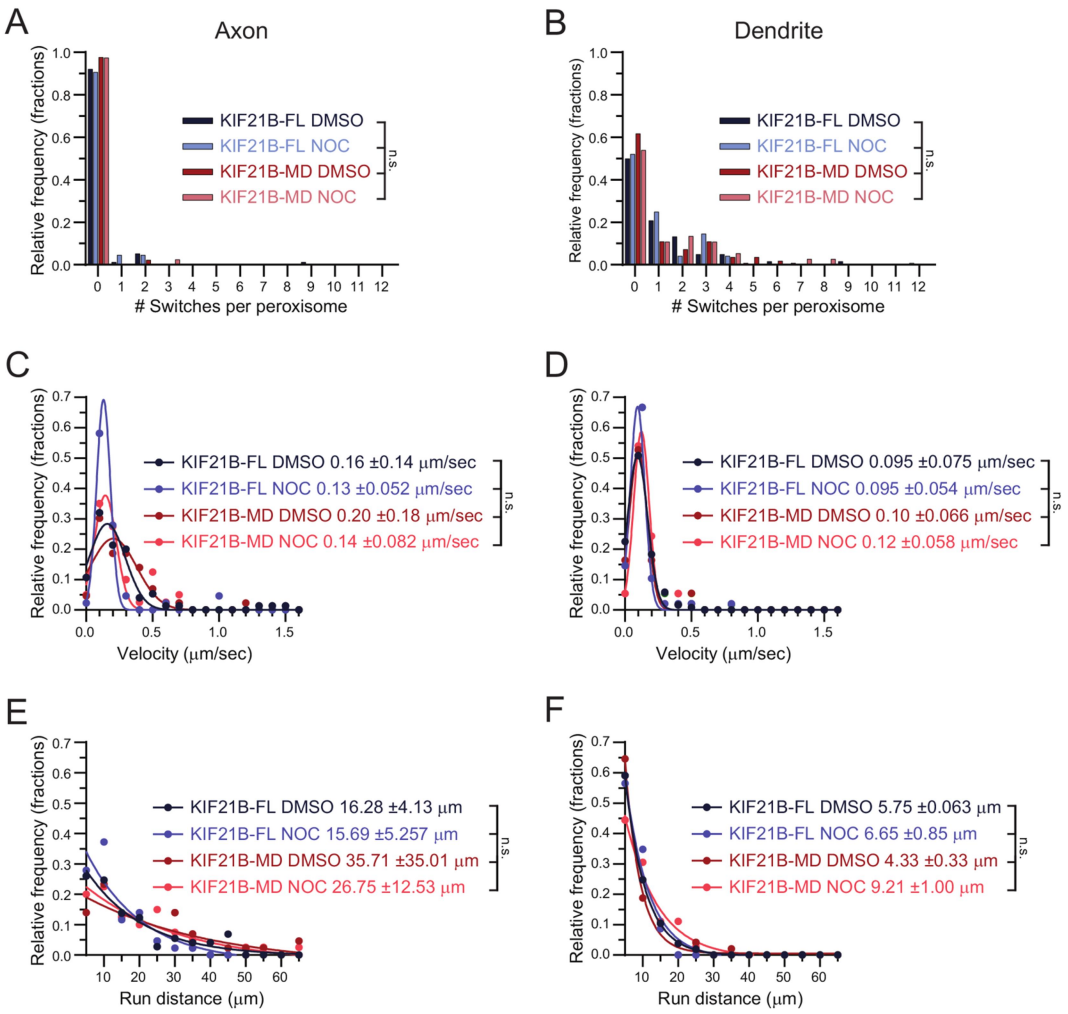

Figure S12. KIF21B induced retrograde trafficking in dendrites requires C-terminal tail domains and MT dynamics. A and B) Histogram of the number of track switches per peroxisome run in axons and dendrites. Motor and DMSO or nocodazole (Noc) conditions are indicated in the graph legend. Track switches are characterized by a reversal in direction

that exceeds 0.4 µm in both anterograde and retrograde directions. Kruskal–Wallis one-way ANOVA and Dunn's multiple comparison (n.s. $p > 0.05$). C and D) Histogram of velocities of motile peroxisomes after photoactivation in axons and dendrites. Motor and DMSO or nocodazole (Noc) conditions are indicated in the legend. Data points were fitted by a gaussian function. Listed are the means and standard deviations for each condition. Kruskal–Wallis one-way ANOVA and Dunn's multiple comparison (n.s. $p > 0.05$). E and F) Histogram of run distances of motile peroxisomes after photoactivation. Motor and DMSO or nocodazole (Noc) conditions are indicated in the legend. Data points were fitted by a single exponential decay function. Listed for each condition is the average distance traveled, as calculated by taking the inverse of the rate constant, and standard deviations. Kruskal–Wallis one-way ANOVA and Dunn's multiple comparison (n.s. $p > 0.05$). Data for KIF21B-FL DMSO is repeated here from Figure 5 for comparison. Unless otherwise stated, data from 37-120 peroxisomes from n = 18-52 neurons and N = 3-6 independent experiments.